Assessment of the strength of kinetic effects of parallel electron transport in the SOL and divertor of JET high radiative H-mode plasmas using EDGE2D-EIRENE and KIPP codes

A V Chankin[1], G Corrigan[2], A E Jaervinen[3], and JET Contributors*

EUROfusion Consortium, JET, Culham Science Centre, Abingdon, OX14 3DB, UK
[1]*Max-Planck-Institut für Plasmaphysik, Garching bei München, Boltzmannstr. 2, 85748, Germany*
[2]*CCFE, Culham Science Centre, Abingdon, OX13 3DB, UK*
[3]*Lawrence Livermore National Laboratory, Livermore, California 94550, USA*

Abstract

KInetic code for Plasma Periphery (KIPP) was used to assess the importance of kinetic effects of parallel electron transport in the SOL and divertor of JET high radiative H-mode inter-ELM plasma conditions with the ITER-like wall and strong nitrogen (N_2) injection. Plasma parameter profiles along magnetic field from one of the EDGE2D-EIRENE simulation cases were used as an input for KIPP runs. Profiles were maintained by particle and power sources. KIPP generated electron distribution functions, f_e, parallel power fluxes, electron-ion thermoforces, Debye sheath potential drops and electron sheath transmission factors at divertor targets. For heat fluxes in the main SOL, KIPP results showed deviations from classical (e.g. Braginskii) fluxes by factors typically ~ 1.5, sometimes up to 2, with the flux limiting for more upstream positions and flux enhancement near entrances to the divertor. In the divertor, at the same time, for radial positions closer to the separatrix, very large heat flux enhancement factors, up to 10 or even higher, indicative of a strong non-local heat transport, were found at the outer target, with heat power flux density exhibiting bump-on-tail features at high energies. Under such extreme conditions, however, contributions of conductive power fluxes to total power fluxes were strongly reduced, with convective power fluxes becoming comparable, or sometimes exceeding, conductive power fluxes. Electron-ion thermoforce, on the other hand, which is known to be determined mostly by thermal and sub-thermal electrons, was found to be in a good agreement with Braginskii formulas, including the Z_{eff} dependence. Overall, KIPP results indicate, at least for plasma conditions used in this modelling, a sizable, but not dominant effect of kinetics on parallel electron transport.

* See the author list of Litaudon et al, Nucl. Fusion **57** (2017) 102001

1. Introduction

Owing to their relatively low ion and electron temperatures, scrape-off layer (SOL) and divertor plasmas in tokamaks are usually considered as collisional, where collisional plasma transport equations, formulated e.g. in [1] can be applied. In one important respect, however, in application to parallel (along magnetic field lines) heat transport, plasma collisionality is often insufficient to justify the use of collisional (also often referred to as 'fluid') equations. It is well known that it is much less collisional high energy super-thermal electrons, with kinetic energies in the range of 5 to $9T_e$, according to [2,3]), which are responsible for the bulk of the electron heat flux. In this paper, expressions 'conductive power flux' and 'heat flux' will be used interchangeably.

Kinetic calculations typically reveal that at the 'hot' (high T_e) end of the flux tube ('upstream', using the nomenclature adopted in SOL and divertor studies, referring to positions upstream of the plasma flow towards material surfaces, typically at the outer midplane) the heat flux is lower than predicted by the Braginskii formula ('heat flux limiting'), while at its 'cold' (low T_e) end ('downstream', near the entrance to the divertor, or inside of the divertor itself, including positions near divertor targets), the heat flux is higher than Braginskii ('heat flux enhancement'), see e.g. review paper [4] where results of several kinetic codes are assembled and compared with theoretical predictions. Kinetic effects are particularly strong during ELMs [5-7], with the electron heat transmission factor at the target plate, γ_e, increasing by an order of magnitude (up to 70) compared to its value 4.5 for strongly collisional plasmas [8]. According to [9], during an ELM the largest contribution to the increase in the total, ion plus electron, heat transmission factor at the divertor target $\gamma = \gamma_e + \gamma_i$ comes from ions (γ_i), while the increase in the inter-ELM periods is attributed mostly to electrons (γ_e), with γ_e rising by factor up to 50.

Due to the presence of high energy non-Maxwellian tails of the electron distribution function, f_e, near the target, kinetic rates of interaction between electrons and neutrals and impurities may increase by a large factor (see e.g. [10-13]). Such effects are however outside of the scope of the present paper, in which the emphasis is put on the ability of super-thermal electrons to create substantial deviations of the electron heat conduction from predictions based on the classical Braginskii formula, and their impact on heat transmission factors γ_e at the divertor target.

KInetic code for Plasma Periphery (KIPP) [14] is a kinetic code for parallel plasma transport in the SOL and divertor. The code is presently 1D2V, with one spatial coordinate (along magnetic field lines) and two velocity coordinates: parallel and gyro-averaged perpendicular velocities. The present version of the code models kinetically only electrons, with the ion background assumed to be taken from elsewhere, e.g. from fluid codes. The code is based on the continuum discretisation finite volume scheme for the Vlasov-Fokker-Planck equation for parallel electron transport, using the operator splitting scheme to separate parallel propagation (free-streaming) and Coulomb collision operations. The code combines an implicit 2^{nd} order scheme for a full non-linear Coulomb collision operator with an explicit 2^{nd} order scheme for the free-streaming. Further details, as well as results of the code benchmarking, can be found in [15] and refs. therein. In the present work KIPP is used to assess the impact of kinetic effects of parallel electron transport on a number of transport coefficients, primarily parallel electron heat conduction coefficient and electron heat transmission factor at the divertor target. Parallel plasma profiles, taken from an EDGE2D-EIRENE (EDGE2D is the plasma part the code package, while EIRENE is the Monte-Carlo solver for neutrals [16-18]) solution simulating inter-ELM

conditions for one of JET high radiation H-mode pulses, are maintained by power and particle sources in KIPP. Kinetic transport coefficients following from steady state KIPP solutions for a number of radial positions in the SOL are compared with EDGE2D fluid coefficients. The particle source in KIPP is implemented by scaling the numerical factor before f_e to achieve the desired density, while the power source is introduced by the f_e's transformation based on the expansion (or contraction) of the velocity grid by some factor (typically very small due to smallness of the time step) and an interpolation of distribution functions onto the original grid, with the subsequent density correction. For a Maxwellian f_e, this produces another Maxwellian with higher (or lower) T_e. Source terms in KIPP are therefore rather homogeneous, without favoring thermal or super-thermal electrons.

Toroidal effects were accounted for in KIPP calculations described here. According to [19], implementation of toroidal effects into 1D (along magnetic field B) conservation equations can be done by introducing variable cross-section of the flux tube and the effect of the mirror force acting on a charged particle. In KIPP, by default cell faces have different cross-sections, proportional to major radius R, which ensures constant magnetic field flux through cell faces, since $B \propto 1/R$ for low beta edge plasmas. Mirror force $-\mu \nabla B \cdot \frac{\mathbf{B}}{B} = \frac{m v_\perp^2}{2R} \frac{\partial R}{\partial s_\parallel}$ also affects perpendicular velocity owing to $\frac{dv_\perp^2}{dt} = -\frac{dv_\parallel^2}{dt}$, following from kinetic energy conservation. No significant impact of toroidal effects on KIPP solutions was found, as was established by comparing KIPP output with and without the inclusion of toroidal effects. It has to be noted that toroidal effects are expected to influence ions much stronger than electrons. Extension of kinetic treatment onto ions is planned in the next version of KIPP.

Section 2 is dedicated to heat carrying electrons (HCE), the notion widely used throughout the paper. They are responsible for the bulk of the parallel electron heat flux. Their characteristic location in the velocity space, as well as their collision mean free paths, are established. The EDGE2D-EIRENE case and KIPP calculations based on its output are described in Section 3. Intrinsic limitations of KIPP, as well as those related to output profiles from the EDGE2D-EIRENE case, read by KIPP, are discussed in section 4. Results of KIPP calculations are presented in section 5. Finally, conclusions from this work are drawn in section 6. Throughout the paper, in figures showing output from KIPP, profiles are plotted in dimensionless KIPP values, unless otherwise stated.

2. Heat carrying electrons (HCE)

The notion of heat carrying electrons (HCE) is critical for understanding kinetic effects of parallel electron heat transport. A number of factors point to high energy electrons as being primarily responsible for the heat flux. Parallel power flux scales with $\mathrm{v}_\parallel m_e \mathrm{v}^2/2 \propto \mathrm{v}^3$, where $\mathrm{v}_\parallel$ and v are parallel and total electron velocities. Lower collisionality of super-thermal electrons contributes to longer collision mean free paths which scale as $\mathrm{v}_\parallel \tau_e \propto \mathrm{v}_\parallel \mathrm{v}^{3/2} \propto \mathrm{v}^{5/2}$, where τ_e - electron collision time. Finally, the number of high energy electrons includes the velocity phase space factor v^2 (for a given $\Delta \mathrm{v}$). Altogether, the factor favouring high energy

electrons is proportional to $v^{7.5}$. Against this acts the exponential decay of the number of high energy electrons $\exp(-m_e v^2/2T_e)$, following from the Maxwellian distribution. The compromise between these factors, according to kinetic calculations, leads to the energy of electrons, most capable of carrying heat, being of order 3-4 v_{th}, where $v_{th} = \sqrt{T_e/m_e}$ is electron thermal velocity.

Fig. 1 shows averaged power flux density $\langle f_e v_\| v^2/2 \rangle$ (the averaging is done for a given absolute velocity v) vs. normalized total electron velocity v/v_{th} calculated in a KIPP case for a strongly collisional non-drifting plasma with a small, 10%, T_e drop (data taken from [15]). The integral of this flux is also shown. This figure is similar to Fig. 1 of [2], or Fig. 7 of [3], slight differences in numbers can be attributed to a more precise collision operator in KIPP. Such a representation of the power flux density and its plots vs. dimensionless absolute velocity will be referred to as electron heat flux density plots in this paper. The disadvantage of this representation is in its concealing the degree of anisotropy of the distribution function in the $(v_\|, v_\perp)$ space. But its big advantage is in the inclusion of the velocity space factor $4\pi v^2$ accounting for the velocity space between the spheres, which better reflects the contribution of high energy electrons. The maximum of $\langle f_e v_\| v^2/2 \rangle$ in Fig. 1 is achieved at $v/v_{th} = 3.45$, corresponding to electron kinetic energy $m_e v^2/2 = 5.95\,T_e$. Negative numbers for lower velocities, $v/v_{th} < 2.53$ are attributed to the force of the parallel electric field $E_\|$ caused by the electron-ion thermoforce: $-eE_\| = 0.71\nabla T_e$ (the numerical coefficient is correct for plasmas with singly charged ions) [1]. This electric field force pulls electrons upstream, towards higher T_e. The critical electron energy for which this power flux becomes negative, $m_e v^2/2 = 3.2\,T_e$, is larger than the average kinetic electron energy $3/2\,T_e$, hence, all thermal electrons, and even electrons with energy twice the average kinetic energy, carry heat in the 'wrong' direction. The effect of the other part of $E_\|$, caused by the parallel electron pressure gradient, is canceled by the effect of the pressure gradient itself.

An estimate for the collision mean free path of HCE requires knowledge of their characteristic parallel and perpendicular velocities. Fig. 2 of [15] shows the 2D contour plot of the power flux density $f_e v_\| v^2/2$ obtained in the same KIPP run as shown in Fig. 1. The maximum of this quantity is achieved at $v_\|=2.74v_{th}$, $v_\perp=1.92v_{th}$, corresponding to a slightly lower kinetic energy, $5.60\,T_e$, than the $5.95\,T_e$ calculated for the maximum of $\langle f_e v_\| v^2/2 \rangle$, the difference should be attributed to the contribution of the velocity space averaging factor $2\pi v_\perp$ in the latter. Using $5.95\,T_e$ as a characteristic HCE energy and fixing the $v_\|/v_\perp$ ratio at 2.74/1.92=1.43, one obtains $v_\|=2.82v_{th}$ and $v_\perp=1.98v_{th}$ as characteristic parallel and perpendicular HCE velocities. Very approximately, using the scaling v^3 for the collision time of super-thermal electrons, and taking into account the difference between the characteristic kinetic energy of HCE, $5.95\,T_e$, and the average electron energy $3/2T_e$, one obtains the factor $(5.95/1.5)^{3/2}$ = 7.90 of increase in the collision time. Taking into account also higher parallel velocity of the HCE, $v_\|=2.82v_{th}$, compared to the parallel velocity of a thermal electron with the parallel energy $T_e/2$:

$v_{\|th} = \sqrt{T_e / m_e} = v_{th}$, the overall factor of increase in the collision mean free path of HCE, which scales as $\tau_{coll} v_{\|}$, becomes 7.90×2.82=22.3.

The above estimate for the characteristic HCE kinetic energy and collision mean free path is very approximate. If, for example, one used the kinetic energy $7.03T_e$, corresponding to the absolute electron velocity at which the integral of $\langle f_e v_{\|} v^2 / 2 \rangle$ reaches half of its maximum, one would have obtained a factor 31.1 increase for the collision mean free path of HCE.

Another issue with making more precise estimates for the collision mean free path of HCE is related to the effect of electron-ion (e-i) and electron-electron (e-e) collisions. Most often, in the literature by electron collision time one assumes the e-i collision time given by (or coinciding with) Braginskii's electron collision time [1]:

$$\tau_e = \frac{3\sqrt{m_e} T_e^{3/2}}{4\sqrt{2\pi}\Lambda_c e^4 Z^2 n_i} \ . \qquad (1)$$

Here Λ_c is Coulomb logarithm, Z is ion charge, and the plasma neutrality, $Zn_i = n_e$, is assumed. When the plasma consists of more than one ion species, a substitution of $Z^2 n_i$ with $Z_{eff} n_e$ in numerical estimates is typically made. The collision time Eq. (1) coincides with 'electron collision time' used in [8].

Super-thermal electrons also collide with thermal electrons. According to [20], for electrons with $m_e v^2 / 2 >> T_e$ parallel slowing down time $\tau_s^{e/e}$ due to their collisions with other electrons is ½ of that for e-i collisions, $\tau_s^{e/i}$, while their perpendicular diffusion time (in velocity space) τ_d, which describes pitch angle scattering, is the same for e-i and e-e collisions (Table 2 of [20]). In addition, e-e collisions, unlike e-i collisions, are very efficient in reducing energy of super-thermal electrons. The characteristic collision time of this process is $\tau_\varepsilon^{e/e} = m_e v^2 / 8T_e \times \tau_s^{e/i}$ (Table 2 of [20]), which for $m_e v^2 / 2 = 6T_e$ is equal to $1.5\tau_s^{e/i}$. Altogether, one can probably assume that the effect of e-e collisions reduces the overall collision time of super-thermal electrons, and hence, their collision mean free path by factor 2 compared to the effect of only e-i collisions. Estimates in the previous paragraph gave for the collision mean free path of HCE the factor 22.3 – 31.1 increase compared to thermal electrons. Owing to the effect of e-e collisions, this factor should be reduced by about a half, giving only the factor 11.2 – 15.6 increase. Taking the average between these two numbers, one may assume that approximately the collision mean free path of HCE can be characterized by factor 13 increase compared to the collision mean free path of thermal electrons. The often used dimensionless collisionality, defined as $\nu^* = \nu_{coll} v_{th} / L_{\|}$, where ν_{coll} is collision frequency calculated as $1/\tau_{coll}$ with the collision time calculated according to Eq. (1), should therefore be reduced by factor ≈ 13 when HCE are considered.

3. EDGE2D-EIRENE case and KIPP runs

Radiative, partially detached operation in JET H-mode plasmas with the ITER-like wall was experimentally investigated and simulated with EDGE2D-EIRENE code package in two divertor configurations [21]. The code cases, without drifts and currents, were ranged according to the divertor configuration (with the outer strike point on the vertical or horizontal target, with the inner strike point being on the vertical target in both configurations), input power into the discharge and nitrogen radiation levels. One of the catalogued EDGE2D-EIRENE cases ('ajarvin/edge2d/jet/85274/feb2116/seq/#3', not listed in the tables in [21]) was chosen to provide the plasma background for KIPP simulations. This case corresponds to the JET discharge with both strike points on vertical targets, 8 MW of input power and 5 MW of nitrogen radiation in a the mostly deuterium plasma. Deuterium radiation, together with a small amount of the radiation on beryllium impurities, was below 0.5 MW. Tungsten radiation at the plasma edge was negligible, for this reason tungsten was not included as an ion species, which consisted of deuterium (D), beryllium (Be) and nitrogen (N) in the simulations. The nitrogen injection levels in EDGE2D-EIRNE cases modelled in [21] are not quoted. This is because nitrogen was assumed as a recycling impurity in the modelling (EDGE2D-EIRENE has only two possibilities: fully recycling or fully absorbing impurity), whereas in reality it is a partly recycling impurity. The N content in the plasma was maintained by 'extra neutral flux' feedbacked on the impurity radiation level (5 MW, as stated above). The amount of this 'extra' flux was 1.5×10^{20}, in electrons per second. Similar to the main (deuterium) neutrals, nitrogen neutrals (N_2) were pumped at the pump surfaces specified in EDGE2D at the rate equal to the 'extra' flux, which indicates that steady state conditions were reached in the modelling case.

For the given discharge parameters, the EDGE2D-EIRENE solution yielded large variations of electron temperature, T_e, along field lines in the SOL/divertor plasma, ranging from 90 eV in the main SOL to below 1eV at target plates. Under these conditions strong contributions of kinetic effects to the parallel electron transport could be expected.

The EDGE2D grid used in the simulation is shown in Fig. 2, and the expanded view of the grid in the divertor region is shown in Fig. 3. The divertor surrounds the part of the grid shown in Fig. 3. Divertor and wall (vacuum vessel) structures are shown in Fig. 1 of [21]. Also shown in Fig. 3 are numbered cells of radial positions indicating poloidal 'rings' (using the nomenclature adopted in EDGE2D, referring to the space in the poloidal cross-section between neighboring flux surfaces) chosen for KIPP runs, which will be referred to below as 'slices' with numbers i from 1 to 6. Fig. 3 also shows arrows indicating the poloidal projection of counting the parallel (along field lines) distance in this paper: from the inner to outer target (opposite to the counting adopted in EDGE2D: from the outer to inner target). Slice i = 1 belongs to the first poloidal ring just outside of the magnetic separatrix. Radial profiles of n_e, T_e and T_i at the outer midplane position from the EDGE2D-EIRENE output are shown in Fig. 5, and target profiles of T_e, n_e and ion saturation current density across target surfaces j_{sat} are shown in Fig. 5. Small T_e around strike point positions and j_{sat} having its maxima outside of these positions indicate partial detachment near strike points.

EDGE2D allows extraction of plasma parameters along parallel direction (along magnetic field lines). The most important parameters extracted at cell centres are electron and ion temperatures and Z_{eff}. Average ion parallel velocities were extracted at cell faces. In addition, for comparison with the KIPP output, parallel electron convective and conductive power fluxes were also extracted at cell faces. During KIPP runs, EDGE2D parameters (input for KIPP) were

maintained by particle and power sources. The most important macroscopic output parameters from KIPP are electron parallel conductive power flux (through cell faces) and ion-electron thermoforce (at cell centres) alongside electron distribution functions, f_e, at cell centres.

KIPP employs a 2nd order scheme for parallel propagation of electrons, which relies on linear interpolations between cell centre and cell face values. For this reason sharp changes in plasma parameters from cell to cell reduce the code accuracy. It was found already in the first runs that smoothness of KIPP output profiles could be increased if the grid shown in Fig. 2, with 88 cells in the poloidal direction, was made finer. As a result, the number of grid cells in the poloidal direction was increased by factor 2, from 88 to 176, by dividing each cell in half and interpolating EDGE2D output profiles from original to new, thinner cells. This led to elimination of some artifacts in KIPP output profiles caused by strongly non-linear features in the input data (output from EDGE2D). Other limitations of KIPP influencing its ability to provide correct output will be discussed in the next section.

Since the EDGE2D-EIRENE case had no parallel currents, ambipolarity of parallel plasma fluxes was assumed. In KIPP this is achieved via adjustments of parallel electric field ($E_{||}$) inside of cells, resulting in equal electron and ion fluxes through cell faces (with ion fluxes being an input from EDGE2D). Ambipolarity at boundary cell faces, adjacent to targets, was achieved by calculations of Debye potential sheath drops which made electron fluxes equal to ion fluxes.

In the EDGE2D-EIRENE case, heat flux limits were used for both ions and electrons, with heat conduction coefficients given by $\kappa_{||}/(1+|q_{||}/q_{fl}|)$, $q_{||}=-\kappa_{||}\nabla_{||}T$, with coefficients $\kappa_{||}$ calculated according to the '21 moment approach'. The electron coefficient $\kappa_{e||}$ was found to be very close to the Braginkii result. Heat fluxes are limited by $q_{fl}=\alpha nT^{3/2}/\sqrt{m}$, with coefficients α set to 10 for both ions and electrons for the case analysed. Coefficients equal to 10 imply a very weak limitation of the theoretical heat flux coefficient applicable to strongly collisional plasmas.

In order to cover the wide range of electron temperatures, a logarithmic velocity grid was used, with 400×200 grid cells (400 for parallel velocity to cover both positive and negative values, and 200 for perpendicular velocity) and an increase in the cell size by factor 1.02 from each cell towards the adjacent cell, at higher absolute velocity, for both parallel and perpendicular velocities. The cell linear size was thus varied by factor ≈ 52, translated into factor ≈ 2700 for electron energies.

KIPP uses dimensionless parameters. Electron velocities, in particular, are normalized by $\sqrt{T_o/m_e}$, with T_o being the highest T_e along a given field line, for each radial position. The maximum parallel and perpendicular velocities of the velocity grid are $7\sqrt{T_o/m_e}$.

Power and particle sources and sinks, aimed at maintaining given (extracted from the EDGE2D-EIRENE solution) parallel profiles, were, as explained in Sec. 1, rather homogeneous across the velocity space, instead of e.g. targeting super-thermal tails for power sinks, for the case of local T_e being << ionization potential of neutral atoms. Implementation of kinetic excitation,

ionization and other rates in KIPP will be done later. In this study, the emphasis is put on the effects of electron parallel transport and Coulomb collisions.

4. Limitations of KIPP

As was already pointed out in the previous section, KIPP runs are subject to a number of limitations. One of them is related to smoothness of parallel profiles of plasma parameters. For this reason, the number of spatial cells in the present study was doubled (see above). In particular, inaccuracies in the linear interpolation of cell centre T_e values on cell faces led to inaccuracies in the calculation of electron conductive power flux, $q_{e,cond}$, which is defined as the total electron power flux q_e minus convective electron heat flux $q_{e,conv} = 5/2\Gamma T_e$, and which is to be compared with EDGE2D-EIRENE and Braginskii conductive power fluxes. Such inaccuracies increase when T_e profiles become strongly non-linear (or, more generally, when the 2nd derivative becomes large). There are also inaccuracies in the calculation of electron particle fluxes through cell faces. In KIPP, electron cell face fluxes have to match ion cell face fluxes taken from EDGE2D. The match, as was pointed out earlier, is achieved by the $E_{\|}$ adjustment, which has to maintain the parallel electron momentum, such that parallel ion velocities in cell centres could be matched. In the presence of strongly non-linear profiles this match cannot be achieved and corrective cell face fluxes have to be used. The ratio of corrective to original fluxes has to be small for the results to be trustable. This ratio is one of the KIPP output parameters after the completion of each time step. Finally, there is some contribution from the Monte Carlo noise, mostly affecting electron density profiles.

Strongly non-rectangular cells, in particular, EDGE2D grid cells around the X-point, present another numerical problem for KIPP whose equations employ the philosophy of a flux tube. When reading EDGE2D-EIRENE output data into KIPP, it is implicitly assumed that an infinitely narrow flux tube passes through centres of EDGE2D cells. In reality, EDGE2D solves equations in flux coordinates, so their reconstruction in the Cartesian coordinate system leads to inaccuracies in the mapping, resulting in wiggles in the profiles. The mapping inaccuracy depends on local change of grid size which is the largest near the X-point. In the future, correcting coefficients for transferring EDGE2D output data to KIPP will be applied, which will generate correct temperature derivatives that must be used in KIPP in order to match EDGE2D and KIPP fluxes.

5. KIPP results

In this section results of KIPP calculations along field lines from the inner to outer target for 6 radial positions ('slices') indicated in Fig. 3 and numbered from 1 to 6 are presented. The positions will be indicated by index 'i' in the rest of the paper. In all these cases dimensionless upstream electron collisionalities ν^*, defined as the ratio of the half of the parallel length from one target to the other, to the electron-ion (e-i) collision mean free path for parameters of the 'hottest' (highest T_e) cell, calculated according to Braginskii's formula Eq. (2.5e) for Z_i=1 [1], were quite similar, varying only between 14.2 and 19.3. Z_{eff} in 'hottest' cells were close to unity for all slices. The division by 2 is required for the direct comparison with formulas in [8], where the parallel length is taken to be the distance between the upstream position and the target. According to [8] (Eq. (4.127), $\nu^* > 15$ gives the condition for a significant T_e drop along the field line. Hence, EDGE2D-EIRENE results analysed here are expected to have only moderate T_e variations along field lines, which is indeed the case for T_e variations in the main SOL plasma,

outside of the divertor. For slices i = 1 to 4, closer to the separatrix, an additional strong T_e drop from the entrance to the divertor down to divertor targets follows from the EDGE2D-EIRENE simulation, which is attributed to strong radiation in the divertor, mostly on nitrogen ions.

For parallel electron heat fluxes (or 'conductive power fluxes') three different quantities will be plotted in the figures: q_{KIPP} from KIPP calculations, q_{EDGE2D} from the EDGE2D-EIRENE output, and q_{Brag}, calculated from the Braginskii formula (1st term on the right hand side of Eq. (2.11) of [1]) for given parallel T_e and Z_{eff} profiles (dependence on Z_{eff} is discussed just below). These conductive power fluxes will be compared with each other. Strong deviations of q_{KIPP} from q_{EDGE2D} and q_{Brag} (the two latter fluxes were found to be close to each other) indicate the importance of kinetic effects in the parallel electron transport. In addition, parallel profiles of convective power fluxes q_{conv}, calculated as $5/2\Gamma T_e$, where Γ is parallel plasma (ambipolar) particle flux and T_e – electron temperature at a cell face, will also be presented. Values of these particle fluxes coincide with the direct output from the EDGE2D-EIRENE case.

Conductive power fluxes q_{theory} for arbitrary Z_{eff} are taken from the Appendix of [22]:

$$q_{e\|,cond} = -\frac{13.58}{Z_{eff}} \frac{Z_{eff} + 0.21}{Z_{eff} + 4.2} \frac{n_e T_e \tau_e}{m_e} \nabla_{\|} T_e . \qquad (2)$$

For $Z_{eff} = 1$ the ratio $\frac{13.58}{Z_{eff}} \frac{Z_{eff} + 0.21}{Z_{eff} + 4.2}$ gives Braginskii's coefficient 3.16.

For ion-electron thermoforce, Braginskii's coefficient 0.71 in the expression $R_T = -0.71 n_e \nabla_{\|} T_e$ for the friction force acting on electrons with ion charge Z_i=1 was replaced with $1.5 \times \frac{Z_{eff} + 0.55}{Z_{eff} + 2.273}$. This coefficient matches Braginskii's coefficients for Z_i = 1 and ∞, and deviates from these coefficients for Z_i = 2, 3 and 4 by less than 1.1%.

Out of 6 slices for which KIPP calculations were carried out, results for only two slices: 1 and 6, are presented in this paper, in sections 5.1 and 5.2, respectively, as they represent two extreme cases of SOL and divertor plasmas. In slice 1, closest to the separatrix, a very large drop of electron temperature from the outer midplane to the targets is seen, with T_e near strike points on divertor targets falling below 1 eV, and with the plasma there becoming partially detached. In contrast, in slice 6, which is in the far scrape-off layer, the T_e drop is quite moderate, and the plasma in the divertors being well attached to the targets. KIPP solutions for other slices, from slice 2 to slice 5, may be considered as transitional between slices 1 and 6.

5.1 KIPP results for slice i = 1

Parallel profiles of the three conductive electron power fluxes: q_{KIPP}, q_{EDGE2D} and q_{Brag}, as well as the profile of the convective electron power flux q_{conv} and electron temperature T_e, are plotted in Fig. 6. Positive power fluxes are directed from the inner to outer target. As was pointed

out in Sec. 3, the number of cells used to plot profiles in Fig. 6 was doubled, compared to the number of cells in the EDGE2D-EIRENE case, to improve smoothness of input profiles for KIPP calculations. The maximum upstream T_e is 90.4 eV, and target T_e are 0.26 and 0.75 eV for inner and outer targets, respectively.

A good agreement between q_{EDGE2D} and q_{Brag} in the main SOL, away from the divertor, can be seen, with q_{KIPP} being smaller than these two fluxes by factor up to ~ 1.5 in the most of the main SOL, indicating heat flux limiting due to kinetic effects. Large spikes in q_{KIPP} at positions of maximum T_e gradients, on the other hand, indicate large heat flux enhancement. The contribution of the convective power flux q_{conv} to the total power flux is low. Very large T_e drops near and at the entrances to divertors do not only reduce the reliability of KIPP results, as discussed in Sec. 4, but also put into question correctness of EDGE2D-EIRENE results. In future tests, similar to the ones described in this paper, or in coupled EDGE2D-KIPP runs, the resolution of the EDGE2D grid may need to be increased in order to avoid very large T_e drops between cells close to the X-point.

Fig. 7 shows various output parameters from the EDGE2D-EIRENE case. Large drops in $n_e(T_e + T_i + m_i V_{i\|}^2)$ towards targets indicate conditions of a partial detachment.

Figs. 8a,b are zoomed versions of Fig. 6, showing the same profiles, but only in the inner and outer divertors, respectively. q_{EDGE2D} and q_{Brag} are almost negligible in both divertors, being much less than q_{KIPP}, whereas convective power fluxes q_{conv} are larger than conductive power fluxes q_{KIPP}. This indicates that even greatly increased kinetic conductive power fluxes q_{KIPP}, by factor 10 or even higher above q_{Brag}, don't strongly increase total electron power fluxes to divertor targets which are dominated by large convective power fluxes q_{conv}.

Figs. 9a,b show electron heat flux density plots (conductive power flux densities vs. dimensionless absolute velocity), in the cells adjacent to outer and inner divertor targets, respectively. In such plots in this study the thermal velocity v_{th} is calculated for the highest T_e upstream, which is used for normalization of velocities in KIPP calculations. This explains why oscillating features on these figures appear at very small dimensionless velocities. Bump-on-tail features on these profiles appearing at $v/v_{th} \approx 3.5$ can also be seen. The total conductive power flux can be calculated by simply integrating the power flux over the value of the X-axis, as is the case of Fig. 1. Such an integration shows that the contribution to the conductive power flux density at outer target, coming from the bump-on-tail feature (see Fig. 9b), is dominant. Non-local electrons responsible for the bulk of the heat flux have energies close to HCE energies of upstream electrons with $v = 3 - 4v_{th}$, hence, they are likely to originate from the region with the highest T_e upstream. At the inner target (Fig. 9a) the contribution of the bump-on-tail feature is less pronounced.

At the entrances to divertors, electron heat flux density plots, shown in Figs. 10a,b, indicate the strong presence of non-local electrons coming from the hottest (with the highest T_e) positions along the field line. In Fig. 10a for the entrance to the inner divertor, their presence manifests

itself as weakly attenuated (by Coulomb collisions) bump-on-tail feature, while in Fig. 10b for the entrance to the outer divertor, they contribute to an extended high energy tail.

In addition to conductive power fluxes, electron kinetic effects are also expected to influence electron-ion (e-i) thermoforce $R_T = -k_T n_e \nabla_\parallel T_e$, where $k_T = 1.5(Z_{eff} + 0.55)/(Z_{eff} + 2.273)$ (see Sec. 5). The e-i thermoforce and the compensating electric field $E_T = k_T \nabla_\parallel T_e / e$ are calculated at each time step during the KIPP run. Parallel profiles of E_T, following from the KIPP calculations and from the theoretical formula using the k_T coefficient above, expressed in internal dimensionless KIPP units, are plotted in the top box of Fig. 11. A fairly good match between the two quantities can be seen in the figure for almost all cells. The bottom box shows thermoforce coefficients k_T calculated using KIPP and the above formula for $k_T(Z_{eff})$, together with the Z_{eff} profile. The horizontal dash-dotted line corresponds to $k_T = 0.71$, the theoretical coefficient for $Z_{eff} = 1$. Coefficients extracted from KIPP results require division by $\nabla_\parallel T_e$, leading to singularities near the T_e maximum. In accordance with a good agreement between KIPP and theoretical values for E_T, a good agreement between the two k_T coefficients can also be seen (except for the singularity feature). Z_{eff} (which is an output from EDGE2D-EIRENE) is close to unity near the targets due to the ion-impurity thermoforce which moves impurity ions upstream. The good agreement between the two E_T profiles, as well as the two k_T profiles, could be expected, since the e-i thermoforce is known to be caused by the friction force exerted on ions mostly by thermal and sub-thermal electrons which are little affected by non-local transport of high energy electrons. Since the good agreement shown here features in KIPP solutions for all slices in this study, such plot won't be shown for slice i = 6 in the next section.

The Debye sheath potential drop coefficients $e\Delta\Phi/T_e$ at the targets, where $\Delta\Phi$ is the Debye sheath drop and T_e is target temperature, are 2.58 and 2.66 for inner and outer targets, respectively, which agrees well with Eq. (2.60) of [8] for target T_i/T_e ratios following from EDGE2D-EIRENE (close to 1 for i = 1). This shows that super-thermal electrons contribute very little to the formation of sheath potential drops. At the same time, electron heat transmission factors $\gamma_e = q_{e,tar}/(\Gamma_{e,tar} T_{e,tar})$, where $q_{e,tar}$ is the total electron power flux through boundary cell faces, $\Gamma_{e,tar}$ is electron particle flux through the sheath, and $T_{e,tar}$ is electron temperature at the sheath (which coincides with the boundary cell face), are 5.17 and 5.28 for inner and outer targets, respectively, which is somewhat higher than according to Eq. (2.90) of [8] for target T_i/T_e ratios close to 1, which follow from EDGE2D-EIRENE. Values close to the theoretical value of 4.8 for strongly collisional plasmas, are not surprising, since electron power flux to the targets is dominated by convection in this slice.

5.2 KIPP results for slice i = 6

Parallel profiles of conductive and convective electron power fluxes, together with the T_e profile, are shown in Fig. 12. Notations are the same as in Fig. 6. The T_e profile shows a rather moderate drop to the targets. Heat flux limiting in the regions of sharp T_e drops is relatively small. The contribution of power convection is larger than for other slices. The maximum upstream T_e is 31.1 eV, and target T_e are 8.26 and 23.48 eV, for inner and outer targets, respectively.

Fig. 13 shows the same output parameters from the EDGE2D-EIRENE case as shown in Fig. 7 for slice i = 1. Flatness of the $n_e(T_e + T_i + m_i V_{i\|}^2)$ profile and a relatively small n_e variation along the field line indicate that the plasma is in a moderate recycling regime with a small momentum loss in the divertor.

Figs. 14a,b are zoomed versions of Fig. 12, showing the same profiles, but only in the inner and outer divertors, respectively. Due to low recycling in this slice, q_{EDGE2D} and q_{Brag} are not too much different from q_{KIPP}. The electron conductive power flux q_{KIPP} is larger than the conductive power flux q_{conv}, which is a consequence of low recycling at the targets.

Electron heat flux density plots are shown in Figs. 15a,b for inner and outer targets, respectively. Both have no bump-on-tail features and look rather similar to that in [3] (Fig. 1) for the case of strongly collisional plasmas. The profile at the inner target shows a somewhat extended tail for higher electron energies, probably due to the stronger T_e drop at the inner target than at the outer target.

Overall, these results, as well as results from slices i = 2 - 5, not presented here, reveal that the heat flux limiting for the analysed EDGE2D-EIRENE case typically doesn't exceed factors ~ 1.5. Flux enhancement factors downstream, on the other hand, may be large, of order 10 or even larger. When this is the case, however, electron heat convection becomes comparable to conduction, or even larger than it, so the impact of electron kinetic effects on the total electron power flux to the target isn't particularly strong. It has to be pointed out, however, that kinetic effects related only to the parallel electron propagation (free-streaming) and Coulomb collisions were included in the KIPP modelling presented in this paper. Higher kinetic rates of electrons interaction with neutrals and impurities, caused by non-Maxwellian tails of super-thermal electrons, might result in such changes of parallel profiles of macroscopic plasma parameters where kinetic effects could become more important.

Debye potential drops at the targets are 2.81 and 2.93 for inner and outer targets, respectively, which are slightly higher than the numbers 2.70 and 2.83 following from Eq. (2.60) of [8], indicating a possible (minor) role of super-thermal electrons in the formation of the Debye sheath. Electron heat transmission factors are 6.25 and 5.60 for inner and outer targets, respectively.

6. Conclusions

Kinetic modelling with KIPP presented in this paper covers wide range of plasma conditions in the SOL and divertor regions, from attached plasmas (at divertor targets) with moderate T_e drops, to high recycling conditions with partial detachment and large T_e drops: from 90 eV upstream to below 1 eV at the targets. KIPP results are in a broad agreement with earlier studies on electron kinetic effects in SOL and divertor plasmas. In particular, they reveal electron heat (conductive power) flux limiting upstream (heat flux is lower than prescribed by Braginskii equations) and flux enhancement (heat flux is higher than according to Braginskii) downstream.

Deviations from Braginskii values in the main SOL, excluding the divertor, were found to be moderate, by factor ~ 1.5. Closer to, and at divertor targets, heat flux enhancement factors at

slices (radial positions) with large T_e drops from upstream to the targets can be of order 10 or even higher. This is attributed to strong non-locality of electron power transport resulting in the appearance of extended tails or bump-on-tail features on electron heat flux density profiles. Such large heat flux enhancement factors however occur under conditions where electron conductive power flux is low due to low T_e, so that electron convective power flux becomes comparable to, or even higher than the convective power flux. This indicates that, at least for the conditions modelled in this paper, kinetic effects of electron parallel transport are not expected to drastically change parallel profiles of plasma parameters in the SOL and divertor, including electron power fluxes at divertor targets. It is therefore likely that present day 2D fluid codes, such as EDGE2D or SOLPS, aren't too far off from reality in predicting divertor conditions, even when simple estimates based on mean free paths of super-thermal electrons point to the strong presence of kinetic effects rendering fluid equations incorrect.

It is important to stress however that a wider range of plasma conditions, e.g. in discharges with a much higher input power than analysed in this paper, including conditions expected in future fusion devices ITER and DEMO, may lead to different results of kinetic studies. Also, the inclusion of a kinetic model for ions, absent in the present work, may result in stronger kinetic effects, in particular for power fluxes to the target. Finally, the modelling described here is not a self-consistent kinetic modelling, since macroscopic plasma parameter profiles were taken from a fluid code EDGE2D. The use of kinetic ionization and excitation rates in a self-consistent kinetic modelling might produce profiles (e.g. profiles with steeper T_e gradients near the target) in which even electron kinetic transport effects (free-streaming) would be stronger than analysed in this work. The present results should therefore be considered as tentative, requiring confirmation under conditions with wider range of plasma parameters as well as extension of the kinetic treatment onto ions and atomic rates.

Acknowledgement
This work has been carried out within the framework of the EUROfusion Consortium and has received funding from the Euratom research and training programme 2014-2018 under grant agreement No 633053. The views and opinions expressed herein do not necessarily reflect those of the European Commission. Discussions with Dr. D.P.Coster are acknowledged.

References

[1] Braginskii S I 1965 'Transport processes in a plasma', *Review of Plasma Physics* Vol. 1, edited by M.A.Leontovich (Consultants Bureau, New York) p.205
[2] Gray D R and Kilkenny J D 1980 *Plasma Phys*. **22** 81
[3] Chodura R 1988 *Contrib. Plasma Phys.* **28** 303
[4] Fundamenski W 2015 *Plasma Phys. Control. Fusion* **47** R163
[5] Pitts R A et *al.* 2007 *Nucl. Fusion* **47** 1437
[6] Tskhakaya D *et al.* 2008 *Contrib. Plasma Phys.* **48** 89
[7] Tskhakaya D *et al.* 2009 *J Nucl. Mater.* **390-391** 335
[8] Stangeby P C 2000, The Boundary of Magnetic Fusion Devices, IOP Publishing, Bristol.
[9] Tskhakaya D 2017 *private communication*
[10] Batishchev O V *et al.* 1997 *Phys. Plasmas* **4** 1672
[11] Popova L *et al.* 2004 *Contrib. Plasma Phys*. **44** 252
[12] Allais F *et al.* 2005 *J. Nucl. Mater*. **337-339** 246
[13] Tskhakaya D 2016 *Contrib. Plasma Phys*. **56** 698
[14] Chankin A V, Coster D P, and Meisl G 2012 *Contrib. Plasma Phys*. **52** 500
[15] Chankin A V and Coster D P 2015 *J. Nucl. Mater*. **463** 498
[16] Simonini R *et al*. 1994 Contrib. *Plasma Phys*. **34** 368
[17] Reiter D 1992 *J. Nucl. Mater*. **196-198** 80
[18] Wiesen S *et al*. 2006 *ITC Project Rep*. http://www.eirene.de/e2deir_report_30jun06.pdf
[19] Zakharov L E and Shafranov V D 1986 'Equilibrium of current-carrying plasmas in toroidal configurations' *Reviews of Plasma Physics* Vol. 11, edited by M.A. Leontovich (Consultants Bureau, New York) p.153
[20] Trubnikov B A 1965, 'Particle interaction in a fully ionized plasma', *Review of Plasma Physics* Vol. 1, edited by M.A.Leontovich (Consultants Bureau, New York) p.105
[21] Jaervinen A E *et al.* 2016 *Plasma Phys. Control. Fusion* **58** 045011
[22] Huber A and Chankin A V 2017 *Plasma Phys. Control. Fusion* **59** 064007
[22] Chankin A V and Stangeby P C 2006 *Nucl. Fusion* **46** 975

Figures

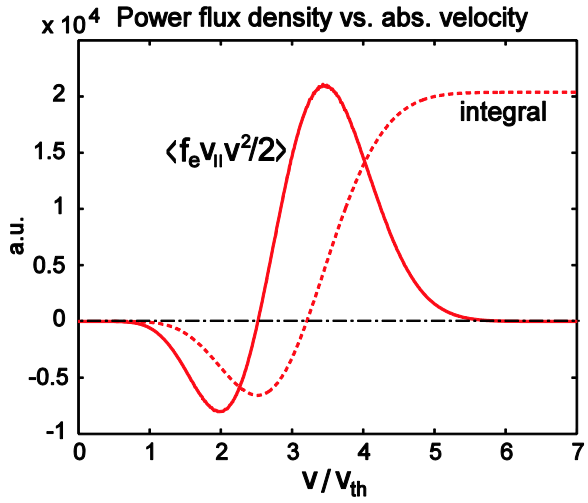

Fig. 1. Electron heat (conductive power) flux density and its integral vs. v/v_{th}, where v is total electron velocity and $v_{th} = \sqrt{T_e/m_e}$, from a KIPP case in a strongly collisional plasma. See text for details.

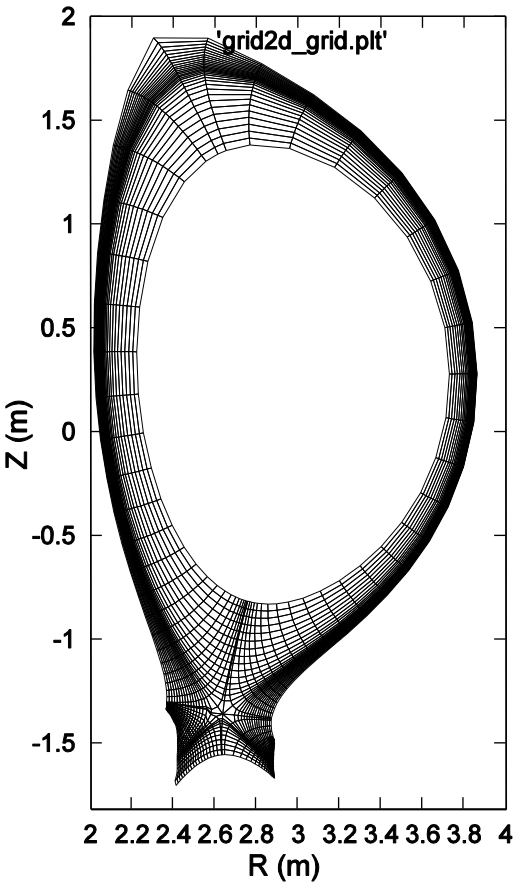

Fig. 2. EDGE2D grid used in the EDGE2D-EIRENE simulation.

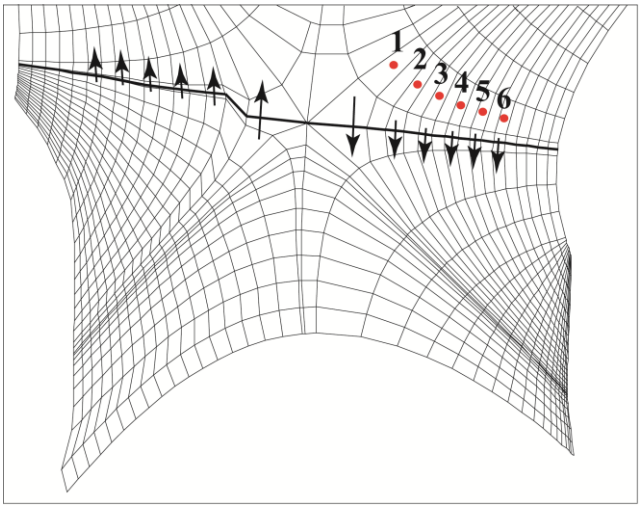

Fig. 3. Expanded view of the EDGE2D grid in the divertor region, showing numbered cells corresponding to radial positions of poloidal 'rings' (using EDGE2D nomenclature) which were chosen for KIPP runs. The chosen rings are referred to as 'slices' (for KIPP runs). Their numbering, given by index 'i' in the paper, doesn't coincide with the ring numbering in EDGE2D.

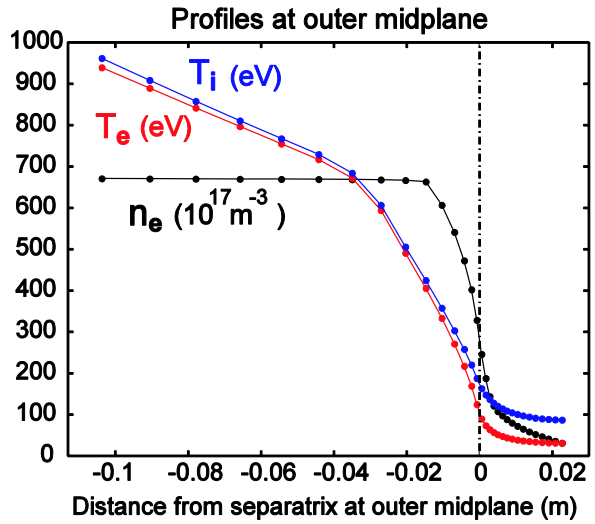

Fig. 4. Ion and electron temperatures and electron density profiles at the outer midplane position from the EDGE2D-EIRENE case vs. distance from the separatrix mapped to the plasma midplane.

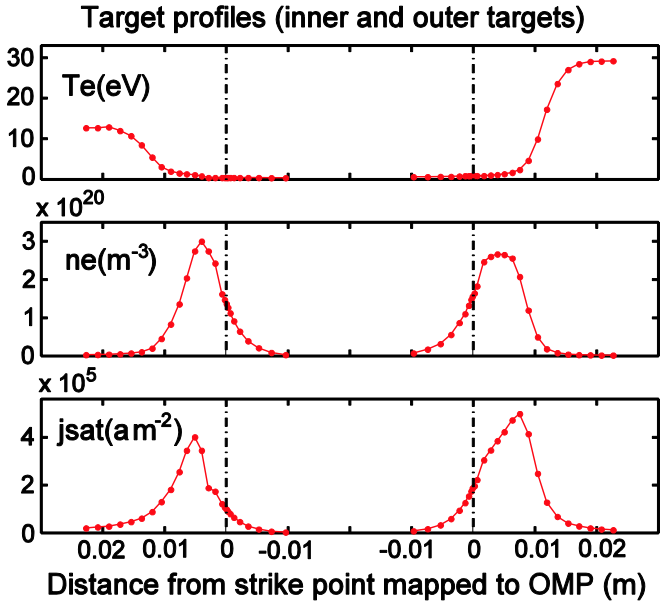

Fig. 5. Target profiles of T_e, n_e and ion saturation current density j_{sat} across target surfaces vs. distance from strike points mapped to the plasma midplane, for the selected EDGE2D-EIRENE case. Vertical dash-dotted lines indicate strike point (separatrix) positions. Positive distances refer to positions in the SOL, negative – to positions in the private flux region.

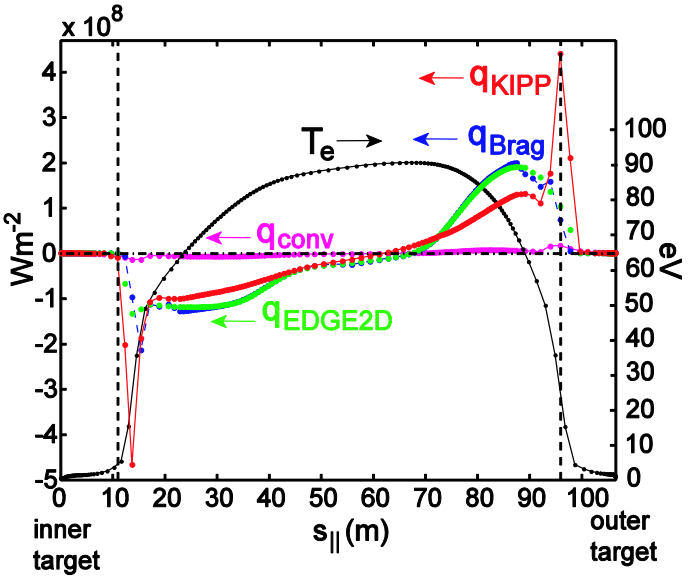

Fig. 6. Parallel profiles of electron conductive power fluxes q_{Brag}, q_{KIPP} and q_{EDGE2D}, together with profiles of electron convective power flux q_{conv} and electron temperature T_e, vs. distance along field lines, from the inner to outer target, for slice i = 1. Vertical dashed lines indicate positions of entrances to the divertor.

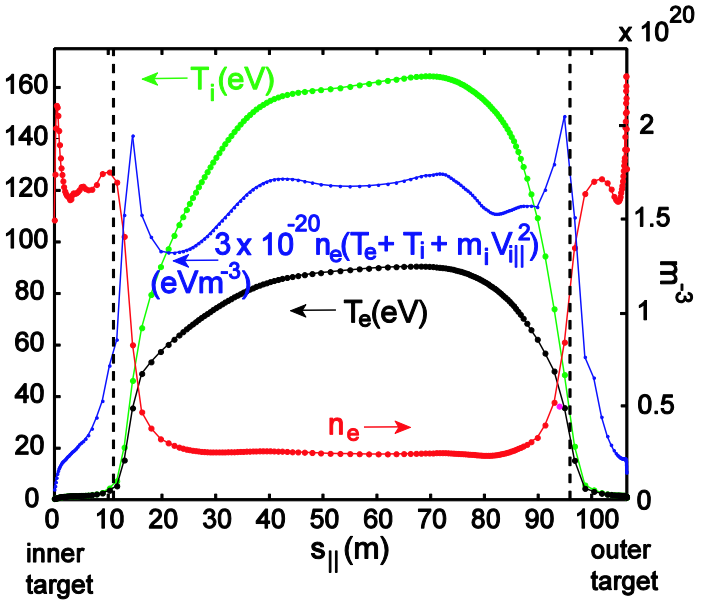

Fig. 7. Parallel profiles of electron and ion temperatures T_i and T_e, the quantity $n_e(T_e + T_i + m_i V_{i\|}^2)$ multiplied by 3×10^{-20}, and electron density n_e, vs. distance along field lines from the inner to outer target, for slice i = 1. Vertical dashed lines indicate positions of entrances to the divertor.

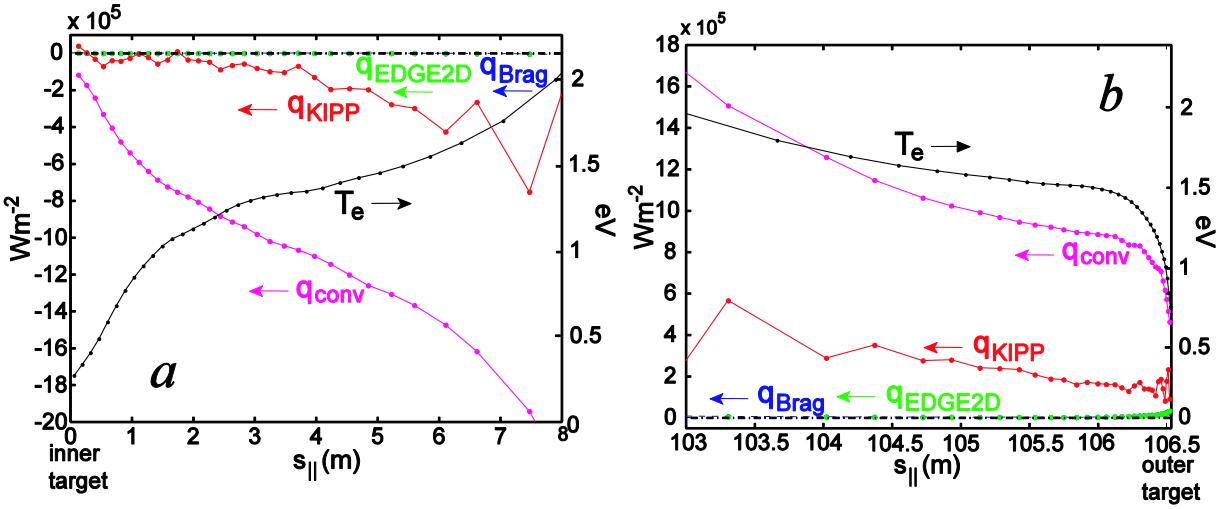

Figs. 8a,b. Same parameters as shown in Fig. 7 (for slice i = 1), but only in the inner (a) and outer (b) divertors.

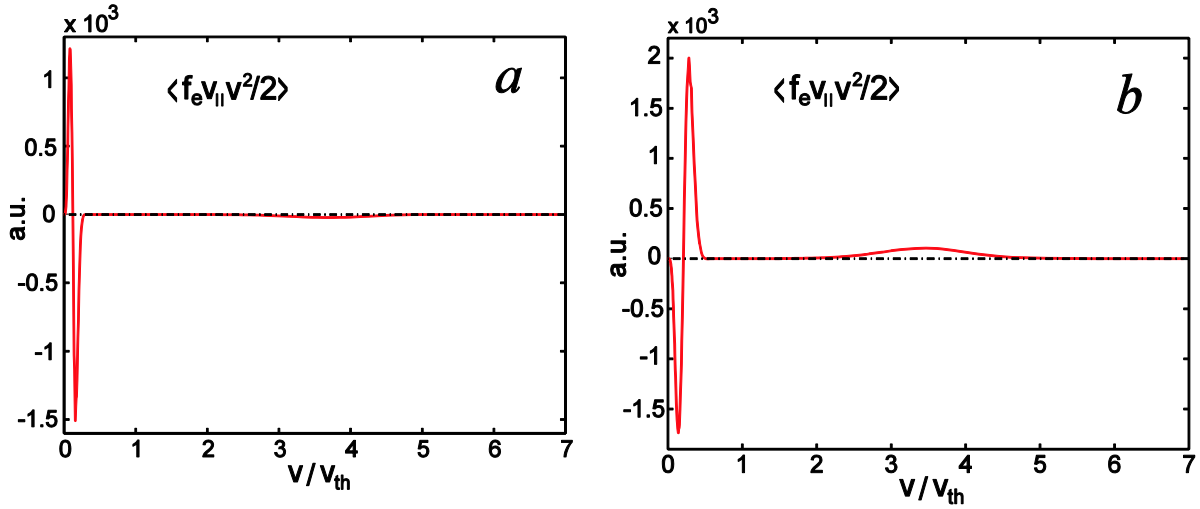

Figs. 9a,b. Electron heat flux density, including the velocity phase space factor, vs. dimensionless absolute velocity, for f_e at cells adjacent to the inner (a) and outer (b) targets, for slice i = 1. Thermal velocity v_{th} is calculated for the highest T_e upstream.

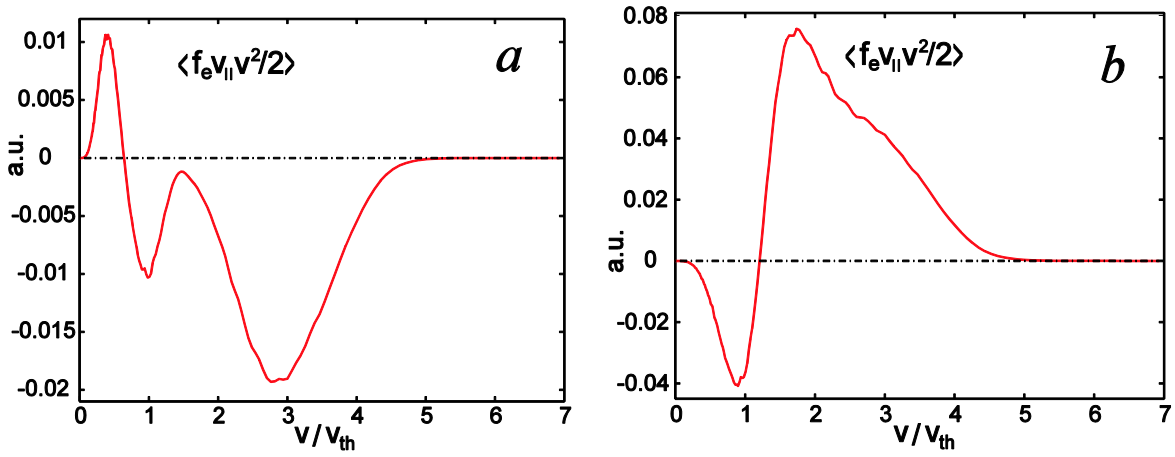

Figs. 10a,b. Electron heat flux density, including the velocity phase space factor, vs. dimensionless absolute velocity, for cells at the entrances to the inner (a) and outer (b) divertors, for slice i = 1. Thermal velocity v_{th} is calculated for the highest T_e upstream. Positions of entrances to divertors are indicated by vertical dashed lines in Fig. 7.

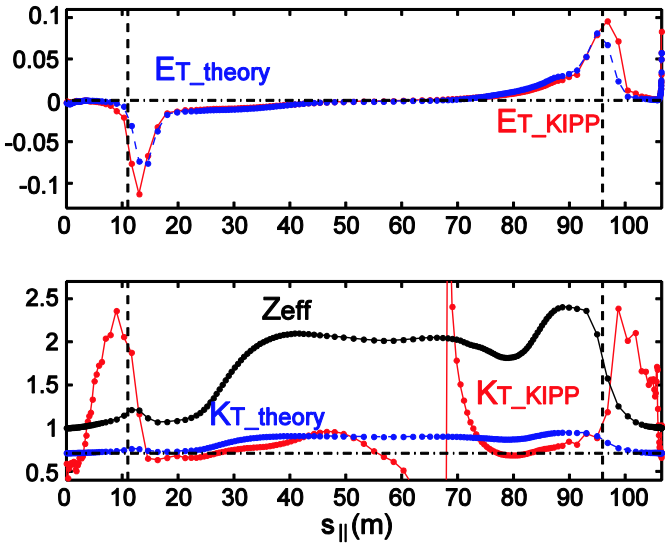

Fig. 11. Parallel profiles of the thermoforce electric field E_T, following from KIPP calculations and from the theoretical formula using the k_T coefficient (top box), and thermoforce coefficients k_T calculated using KIPP and the formula for $k_T(Z_{eff})$, together with the Z_{eff} profile (bottom box), for slice i = 1. The horizontal dash-dotted line in the bottom box corresponds to $k_T = 0.71$.

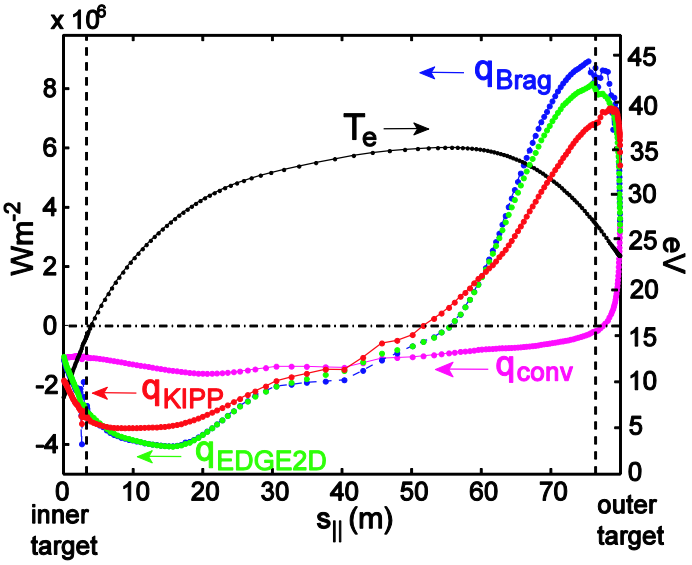

Fig. 12. Parallel profiles of electron conductive power fluxes q_{Brag}, q_{KIPP} and q_{EDGE2D}, together with profiles of electron convective power flux q_{conv} and electron temperature T_e, vs. distance along field lines, from the inner to outer target, for slice i = 6. Vertical dashed lines indicate positions of entrances to the divertor.

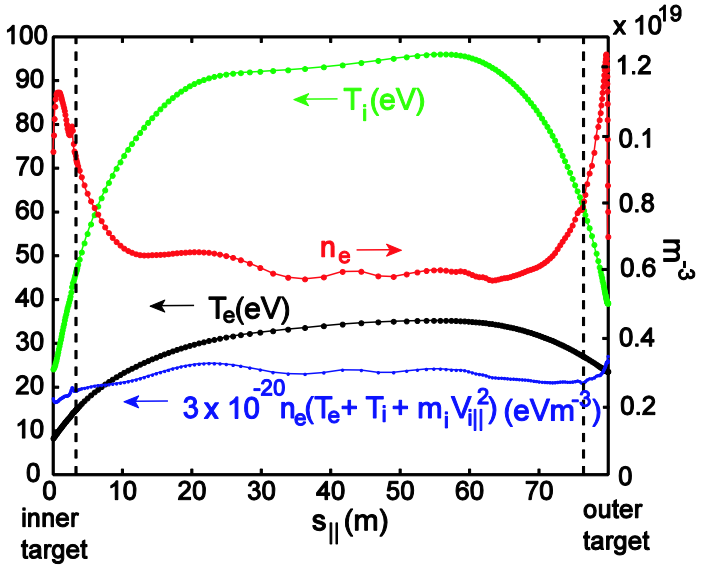

Fig. 13. Parallel profiles of electron and ion temperatures T_i and T_e, the quantity $n_e(T_e + T_i + m_i V_{i\|}^2)$ multiplied by 3×10^{-20}, and electron density n_e, vs. distance along field lines from the inner to outer target, for slice i = 6. Vertical dashed lines indicate positions of entrances to the divertor.

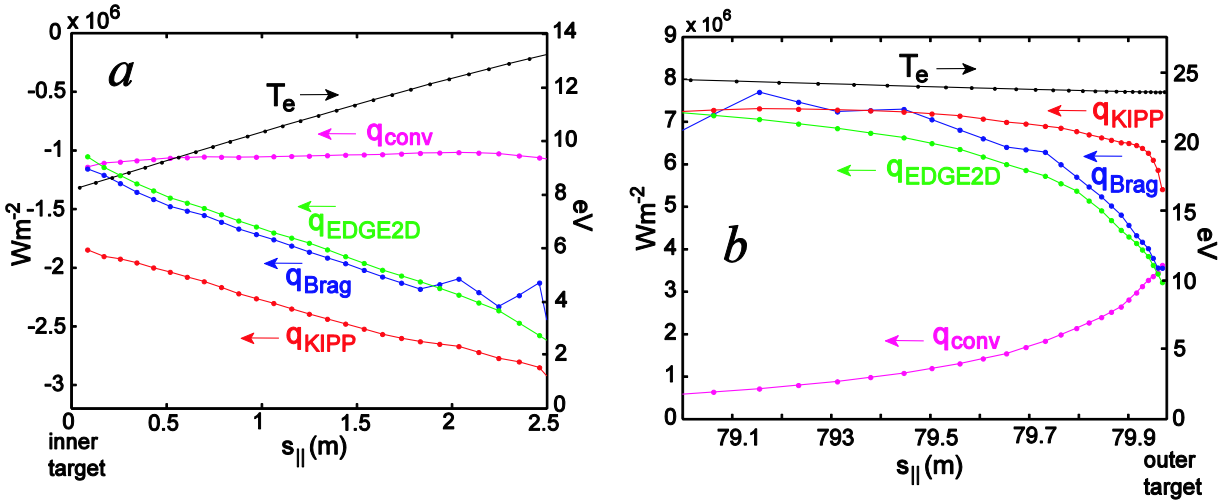

Figs. 14a,b. Same parameters as shown in Fig. 13 (for slice i = 6), but only in the inner (a) and outer (b) divertors.

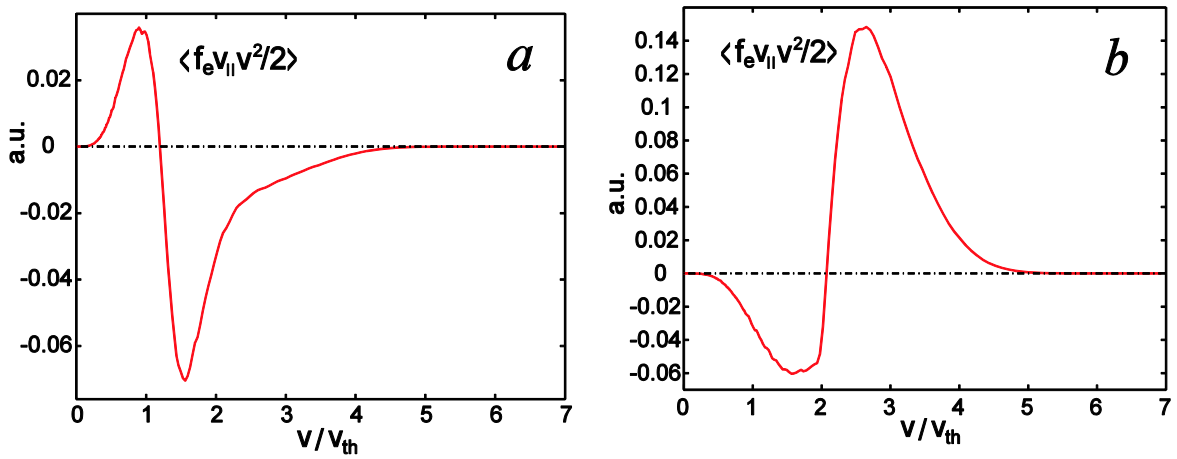

Figs. 15a,b. Electron heat flux density, including the velocity phase space factor, vs. dimensionless absolute velocity, for f_e at cells adjacent to the inner (a) and outer (b) targets, for slice i = 6. Thermal velocity v_{th} is calculated for the highest T_e upstream.